Supporting information for

Unraveling the dynamic behaviors of BF_4-based ionic liquids at $SnO_2/FAPbI_3$ interface by Ab initio molecule dynamic simulations

Jinge Han,[a] Hongbin Xiao,*[a,b] Yanru Guo,[a] Xue Liu,[a] Zhigang Zang,[a] and Ru Li*[a]

[a]Key Laboratory of Optoelectronic Technology & Systems (Ministry of Education), College of Optoelectronic Engineering, Chongqing University, Chongqing 400044, China.
[b]School of Chemistry and Chemical Engineering, Chongqing University, Chongqing 401331, China.

*Corresponding author: xiaohongbin@cqu.edu.cn; ru.li@cqu.edu.cn

Simulation methods:

Ab inito molecular dynamic simulations: the AIMD simulations are performed by the open source code CP2K[1] in the constant-volume and constant-temperature (NVT) ensemble. The temperature was controlled with a conical sampling through velocity rescaling (CSVR) thermostat at room temperature (300 K). The time step was set to 1.0 fs. A PBE-D3 functional was used with double-zeta basis sets (DZVP-MOLOPT) and Goedecker–Teter–Hutter pseudopotentials.[2] The cut-off and real-cutoff were set to 500 Ry and 55 Ry, respectively. The AIMD simulations were run for approximately 10 ps to ensure equilibrium. For the SnO_2 (110) surface, a 25 Å vacuum in the *z* direction was used. A 3×3×3 supercell with one oxygen vacancy defect is constructed. The sizes of the simulation box are 20.5019 Å×12.9729 Å×37.895 Å. The initial geometry is to place one BF_4^- anion above the oxygen vacancy of SnO_2 with a distance of 3 Å. The BF_4^- anion is placed under the cation of the ionic liquid (IL), facing the SnO_2 surface. For the $FAPbI_3$ side, a 3×3×3 supercell (001) surface with the FA terminated morphology is used. The sizes of the simulation box are 19.0839 Å×19.0839 Å×38.6259 Å and the vacuum thickness in the *z* direction is 25 Å. One FA vacancy is created for the AIMD simulation and the IL molecule is placed above the $FAPbI_3$ surface with a distance of 3 Å. To model the iodine migration energy barrier, we created the iodine vacancy close to the FA vacancy, where it was occupied by the IL residues. To explore the influence of the initial configuration of IL on the dynamic behaviors of the BF_4 anion, we rotate the $BMIMBF_4$ by 180°. VMD package is used to visualize the trajectory produced by AIMD simulations.[3]

Density of state (DOS) calculations: the DOS calculations are carried out by the open source code Quantum Espresso v7.2,[4] the SSSP Efficiency (v 1.2.1) pseudopotentials[5] are used to optimize the structure produced by CP2K AIMD simulations until the force is less than 10^{-4} Ry. During the SCF calculation, the ecutwfc cutoff of 80 Ry and energy convergence of 10^{-8} Ry are set. The automatic K points 1×2×1 is used to sample the Brillouin zone.

Electronic static potential: the structure of the ILs are optimized by Gaussian 09 at the b3lyp/6-311+g(d,p) level with DFT-D3, and the minimum of the BF_4^- terminal group in these ILs is obtained with the help of Multiwfn code.[6]

Iodine ion migration: the ion migration energy barrier is calculated by the CI-NEB method that is implemented in the CP2K code. The structure before and after the ion migration is first optimized, and the number of replica is set to 5 and the k-spring is set to 0.05. The convergence criteria are MAX_FORCE less than 0.003, RMS_FORCE less than 0.005, MAX_DR less than 0.002 and RMS_DR less than 0.005.

Table S1. The cation-anion distance of $BMIM^+BF_4^-$, $ICy^+BF_4^-$ and $DHIM^+BF_4^-$.

Molecule	$BMIM^+BF_4^-$	$ICy^+BF_4^-$	$DHIM^+BF_4^-$
Cation-anion distance (Å)	3.12090	3.28038	3.70598

Table S2. Formation energy of different SnO_2 surfaces.

Surface	(100)	(110)	(111)
Energy (eV/atom)	-5.833	-5.935	-5.861

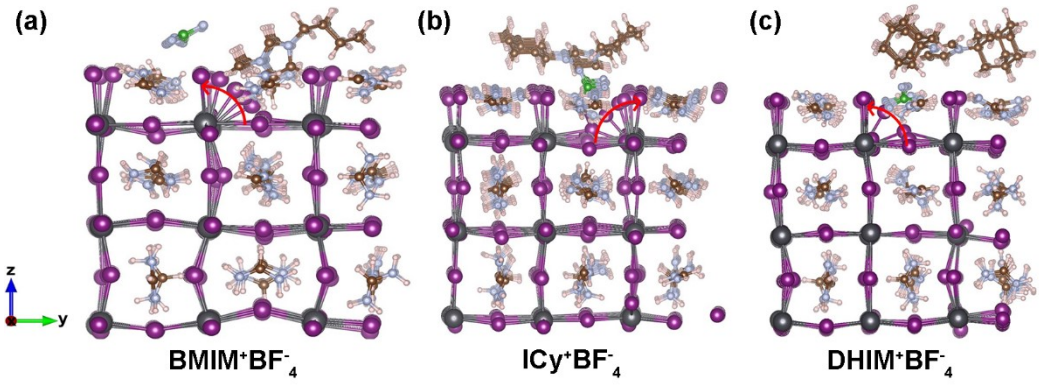

Figure S1. Iodine ion migration path when $BMIM^+BF_2$ (a), ICy^+BF_3 (b) and $DHIM^+BF_3$ (c) residues get absorbed on the FA vacancy of the $FAPbI_3$ (001) surface. The red arrow shows the trajectory of the iodine ion migration path.

Reference:

1. T. D. Kuhne, M. Iannuzzi, M. Del Ben, V. V. Rybkin, P. Seewald, F. Stein, T. Laino, R. Z. Khaliullin, O. Schutt, F. Schiffmann, D. Golze, J. Wilhelm, S. Chulkov, M. H. Bani-Hashemian, V. Weber, U. Borstnik, M. Taillefumier, A. S. Jakobovits, A. Lazzaro, H. Pabst, T. Muller, R. Schade, M. Guidon, S. Andermatt, N. Holmberg, G. K. Schenter, A. Hehn, A. Bussy, F. Belleflamme, G. Tabacchi, A. Gloss, M. Lass, I. Bethune, C. J. Mundy, C. Plessl, M. Watkins, J. VandeVondele, M. Krack, and J. Hutter, J Chem Phys 152 (19), 194103 (2020).
2. Joost VandeVondele and Jürg Hutter, The Journal of Chemical Physics 127 (11), 114105 (2007).
3. William Humphrey, Andrew Dalke, and Klaus Schulten, Journal of molecular graphics 14 (1), 33 (1996).
4. P. Giannozzi, O. Andreussi, T. Brumme, O. Bunau, M. Buongiorno Nardelli, M. Calandra, R. Car, C. Cavazzoni, D. Ceresoli, M. Cococcioni, N. Colonna, I. Carnimeo, A. Dal Corso, S. de Gironcoli, P. Delugas, R. A. DiStasio, A. Ferretti, A. Floris, G. Fratesi, G. Fugallo, R. Gebauer, U. Gerstmann, F. Giustino, T. Gorni, J. Jia, M. Kawamura, H. Y. Ko, A. Kokalj, E. Küçükbenli, M. Lazzeri, M. Marsili, N. Marzari, F. Mauri, N. L. Nguyen, H. V. Nguyen, A. Otero-de-la-Roza,

L. Paulatto, S. Poncé, D. Rocca, R. Sabatini, B. Santra, M. Schlipf, A. P. Seitsonen, A. Smogunov, I. Timrov, T. Thonhauser, P. Umari, N. Vast, X. Wu, and S. Baroni, Journal of Physics: Condensed Matter 29 (46), 465901 (2017).
5. Gianluca Prandini, Antimo Marrazzo, Ivano E. Castelli, Nicolas Mounet, and Nicola Marzari, npj Computational Materials 4 (1), 72 (2018).
6. Tian Lu and Feiwu Chen, Journal of Computational Chemistry 33 (5), 580 (2012).